Mechanical Systems and Signal Processing 132 (2019) 441–456

Contents lists available at ScienceDirect

Mechanical Systems and Signal Processing

journal homepage: www.elsevier.com/locate/ymssp

Enhancement of vibration based energy harvesting using compound acoustic black holes

Hongli Ji [a,1], Yukun Liang [a,1], Jinhao Qiu [a,*], Li Cheng [b], Yipeng Wu [a]

[a] State Key Laboratory of Mechanics and Control of Mechanical Structures, Nanjing University of Aeronautics and Astronautics, Nanjing, China
[b] Department of Mechanical Engineering, Hong Kong Polytechnic University, Hung Hom, Kowloon, Hong Kong

ARTICLE INFO

Article history:
Received 1 February 2019
Received in revised form 5 June 2019
Accepted 28 June 2019

Keywords:
Acoustic black hole
Energy harvesting
Piezoelectric patches

ABSTRACT

Acoustic black hole (ABH) effects can be obtained via proper structural tailoring to induce a gradual reduction of the flexural wave velocity, thus creating high energy density structural areas. The wave energy focalization effect shows promising features for establishing novel vibration energy harvester configurations in terms of the high energy level and broadband characteristics. In this study, an energy harvesting structure with ABH features which ensures the structural strength as well as enhances the harvesting performance is proposed and investigated. Considering the wavelength compression in ABHs, piezoelectric patches bonded on the surfaces of ABHs are sliced into micro arrays to convert the mechanical energy effectively, which make sure that the positive and negative electric charge generated on the surfaces of harvesters won't be neutralized. Each of the transducers is shunted with a resistor impedance. Fully coupled numerical models which consist of vibrational structures and electrical circuits are built to assess the energy harvesting performance of ABH-feature beam and uniform beam under both steady state and transient excitations. Experiments are also conducted to verify the significant performance enhancement in the ABH beam as compared that in the uniform beam. It is shown that the ABH structural tailoring can be used for broadband vibration energy harvesting and boost the harvested power by more than one order of magnitude.

1. Introduction

In recent years, a great research interest has been evoked to reveal the so-called 'acoustic black hole' effect and exploit the mechanism for developing lightweight and highly-damped structures for vibration and noise control. ABHs employ a local thickness decrease according to a power-law profile (in the form $h(x) = \varepsilon x^m$, $m \geq 2$, as shown in Fig. 1) to reduce the local phase velocity of incident flexural waves and the time required to reach the edge becomes infinite if the residual thickness approaches zero [1]. Therefore, waves become trapped at the tip end and do not reflect black in the ideal scenario. It is however shown that the local thickness would never reach zero due to manufacturing difficulties and even a very small truncation can result in high reflection coefficients, making the ABH effect unattractive in practical applications [2,3]. Nevertheless, Krylov et al. show that applied damping treatments can compensate the undesirable effect of truncations and exhibit excellent vibration suppression performances [4,5].

* Corresponding author.
E-mail address: qiu@nuaa.edu.cn (J. Qiu).
[1] These authors contributed equally to this work and should be considered co-first authors.

https://doi.org/10.1016/j.ymssp.2019.06.034
0888-3270/

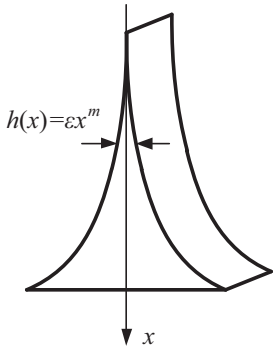

Fig. 1. Elastic wedge of power-law profile.

Owing to the satisfactory flexural waves attenuation abilities, the ABH concept exhibits potential for mechanical vibration and sound radiation control [6–11]. ABHs along with adhesive material can be integrated into existing structures such as airframe and vehicles to act as effective energy dissipation components [12–14]. The reduced wave speed and increased vibration amplitude leads to high strain energy in tapered areas, which is also significant for vibration energy harvesting.

Up to now, most of researches predominantly focus on vibration and noise control, but less on energy harvesting. In the latter category, a representative work is the one on energy harvesting performances of a beam with five embedded one dimensional ABH features [15], with results showing an obvious energy harvesting efficiency. Besides, experiments were conducted on a plate-like structure with three embedded 2D ABHs to investigate the harvesting performance [16]. However, to our best knowledge, all these studies did not take into account the wavelength compression effect in ABH features, as well as the scale of transducers was not designed appropriately, which may fail to convert the energy effectively. When a flexural wave propagates towards the central zones of ABHs, its wavelength is compressed and becomes much less than the scale of ABHs especially at high excitation frequencies. Under bending vibration conditions and neglecting the shear effects, the strain tensor of the same side surface corresponding to peaks and troughs of waves can have opposite phase, resulting in opposite potential polarities since the transducers are polarized normal to the bonding surfaces. Therefore, the positive and negative charge generated on the surfaces of piezoelectric patches may be neutralized, which may dissipate to some extent electricity generation from waves. So the wavelength compression effect need to be considered in the sensor design, which is vital important for better harvesting performance of ABH structure. In addition, literature review also shows that the strong coupling between the add-on elements (transducers, electrical circuits) and the host structure, which can influence the ABH effect, were not taken into account.

In terms of engineering applications, the design issue of effectively producing the ABH effect while ensuring its mechanical property of the structure also needs to be tackled before the ABH technique can find its real engineering application. The conventional ABH structure with small residual thickness can lead itself to issues such as high stress concentration and fatigue failure, which is less likely to be used in practice. Although the ABH effect exhibits outstanding potential for energy harvesting, for now, limited effort has been devoted to improve both properties of the ABH effect and mechanical performance. Therefore, it is needed to explore designs of structures towards more effective energy trapping and conversion while ensuring mechanical properties of the overall structure, as well as to investigate the issue and to gain physical insights into the underlying mechanisms of ABH-specific features under a fully coupled vibro-energy harvesting context.

The goal of this paper is twofold: to propose an energy harvesting structure with ABH features which ensures the structural strength as well as enhances the harvesting performance; and to explore and understand the underlying physics mechanisms and the coupling between the harvesting system and the host structure. To this end, a beam with three one-dimensional double-layered compound ABHs coupled with piezoelectric patches and harvested resistor is investigated. Considering the wavelength compression in ABHs, piezoelectric patches bonded on the surfaces of ABHs are sliced into micro arrays to convert the mechanical energy effectively, which make sure that the positive and negative electric charge generated on the surfaces of harvesters won't be neutralized. The paper is organized as follows: The propagation of flexural waves in tailored wedges is introduced. Then, the configuration of the energy harvesting system is discussed in detail. Each energy harvesting circuit is simplified as a resistor impedance respectively. The harvested power under both transient and steady state excitations are discussed and estimated. Dynamic analyses are also conducted on systems with different transducers to research the influence of the dimension of piezoelectric patches. Experimental verifications are also presented to assess the effectiveness of ABH systems for energy harvesting.

2. Energy harvesting based on the ABH effect

2.1. Propagation of flexural waves in tailored wedges

The equation describing the bending motions of a thin beam in vacuum can be written as [2]:

$$\frac{\partial^2}{\partial x^2}\left[D(x)\frac{\partial^2 w}{\partial x^2}\right]+\rho h(x)\frac{\partial^2 w}{\partial t^2}=0 \tag{1}$$

where w is the transverse displacement of the median plane of the beam, $D(x)=Eh^3(x)/12(1-\mu^2)$ is the local flexural stiffness, E and μ are Young's modulus and the Possion's ratio, ρ is the density, $h(x)$ is the local thickness of the beam.

Neglecting the rotary inertia and the shear effects, the local wave number of the flexural wave in the beam with variable thickness can be written as [17]:

$$k=\left(12\rho(1-\mu^2)\omega^2/Eh^2(x)\right)^{1/4} \tag{2}$$

where $\omega=2\pi f$ is the circular frequency.

Since $c=\omega/k$, the speed of bending wave can be written as:

$$c=\sqrt{\omega h}\left[\frac{E}{12\rho(1-\mu^2)}\right]^{1/4} \tag{3}$$

Substitution of Equation into $\lambda=2\pi c/\omega$ yields:

$$\lambda=2\pi\sqrt{\frac{h}{\omega}}\left[\frac{E}{12\rho(1-\mu^2)}\right]^{1/4} \tag{4}$$

Based on Eqs. (2)–(4), for a homogeneous isotropic flat structure of constant thickness, the phase velocity is proportional to the square root of the frequency. While for a beam with varying thicknesses, it also depends on its local thickness. The thickness-dependent feature of the phase velocity makes it possible to modulate wave propagation by means of local variation of the plate's thickness, which results in dramatic increment of the energy density of the local area. It should be noted that when the frequency is very high and the structure thickness is very thin, the wavelength will become very short due to the compressibility of the bending wave. In this case, the size of the piezo-sensor in the energy harvesting system needs to match the wavelength size, which will be detailed in the following section.

2.2. Energy harvesting in ABH tailored beams

2.2.1. Configuration of the energy harvesting system

In this work, a compound double-layered ABH beam as shown in Fig. 2 was used as the mechanical structure for piezoelectrical energy harvesting. Our previous studies have shown that the compound ABHs structure outperform the traditional ABH structure at both of the static properties of structural strength and rigidity and the dynamic properties of energy focalization [18], which makes it possible to use as practical energy harvester. In order to further increase the modal density and enhance the energy concentration effect, three equally spaced double-layered compound ABHs are embedded in the primary beam-like structure. The beam is forked into the upper and bottom branches in the ABH region with a tapered thickness, symmetrical with respect to the center of the ABH region, x_p. The length of an ABH is l from x_1' at the left end to x_1 at the right end, with tapered regions from x_1' to x_0' and x_0 to x_1 and a platform of constant thickness h_0 from x_0' and x_0. The basic geometry of an ABH from x_p to x_2 is shown in Fig. 2(d), with its thickness defined by $h(x)=\varepsilon(x-x_0)^m+h_0$ from x_0 to x_1 and a constant thickness of h_0 from x_p to x_0.

Six 1-by-14 linear arrays of rectangular piezoelectric patches are bounded on the upper and lower surfaces of each ABH respectively, as depicted in Fig. 3. Considering the wavelength compression of the ABH effect, piezoelectric patches are sliced into small separate pieces in order to avoid the charges generated being neutralized. All the bounding surfaces of piezoelectric patches are set to be ground as boundary conditions in the electrical module. Each transducer is shunted with an individual resistor for harvesting energy.

The piezoelectric patch can be expressed by a current source I_{eq} in parallel with an equivalent capacitance C_p [19], as shown in Fig. 4. For simplicity, each PZT patch employs a pure resistor R as the energy harvesting circuit herein. The AC approach is an effective method to assess the energy harvesting performance of the presented structures and has been used in many studies [15,20–26]. It should be noted that the harvesting efficiency could be further improved by use of more advanced electronic interface circuits.

Under harmonic excitations, the output voltage of the piezoelectric patch, U, the load resistor can be expressed as:

$$U=I_{eq}R/(1+j\omega C_pR)=j\omega QR/(1+j\omega C_pR) \tag{5}$$

where Q represents the amplitude of electric charge on the electrode, which is proportional to the strain, and C_p is the equivalent capacitance of the piezoelectric patch. The harvested power is:

$$P=UU^*/2R=\frac{\omega^2RQ^2/2}{1+(\omega C_pR)^2} \tag{6}$$

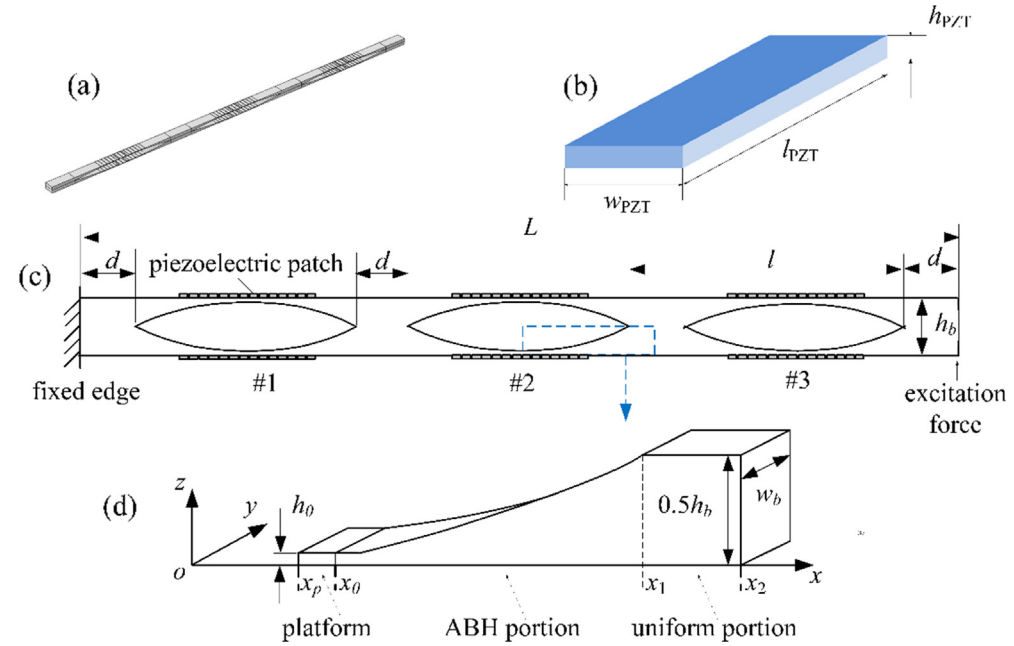

Fig. 2. Beam with three embedded compound ABHs: (a) 3D finite element model, (b) piezoelectric patch, (c) 2D schematic of the profile of the beam, (d) the basic geometry of the lower branch.

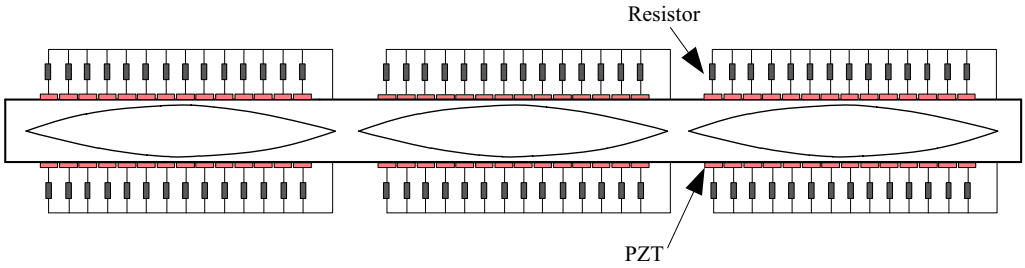

Fig. 3. Schematic of the energy harvesting system.

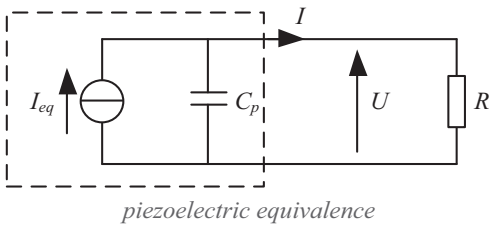

Fig. 4. Standard AC.

2.2.2. Numerical models

The crucial issue of the coupling between the ABH and the piezoelectric patch is not well considered in previous energy harvesting models. The numerical model in this paper is comprised of a mechanical structure and harvesting circuits. A uniform beam of the same dimensions as the ABH beam, bonded the same number and scale of piezoelectric patches, was used for performance comparison, which represents a traditional situation. In the finite element analyses, the left-hand side edges of both the ABH beam and the reference structure are fixed and the external excitation is applied at the free end of the test article in each numerical model.

In order to analyze the vibration response and evaluate the electrical power output of two different configurations, three-dimensional fully coupled numerical models were built and solved using COMSOL. All the piezoelectric patches are assumed to be perfectly bonded with host structures and placed at the same position for both the uniform and ABH beams. Beams and piezoelectric patches are discretized by 3D quadratic block elements. Nodal positions between the beam and PZT patches are set to coincide in order to ensure the displacement continuity and strain compatibility. Since the element size setting is of great importance to the modelling accuracy, the geometric entities especially in tapered areas are meshed fine to ensure more than ten elements per wavelength at the highest frequency of interest. Geometrical and material properties of the ABH beam as well as piezoelectric patches used in the simulation are given in Tables 1 and 2.

Each node of piezoelectric element has three mechanical degrees of freedom (DOFs) and an electrical potential DOF. For modelling purposes, the potential DOFs on the bonding surfaces are grounded as boundary conditions and those on the free electrode surface of each piezoelectric patch are reduced such that only one master potential DOF remains on the free electrode per patch [20]. Hence, the terminals of resistors can be easily connected to the electrodes of transducers respectively to build a fully coupled system.

Piezoelectric patches are polarized in z direction normal to the bonding surfaces. This enables transducers to work in mode 31 where the strain is generated in x direction due to transverse vibrations while the voltage is obtained from perpendicular direction. Considering flexural vibrations which dominate the dynamic response of the system herein, the free electrode surfaces corresponding to peaks would be in tension while that of troughs are in compression, generating charge of different electrical polarities. If the dimension of piezoelectric patches in x direction is larger than the half-wavelength in ABH areas, the positive and negative charge will be neutralized, which directly leads to reduced effectiveness of energy harvesting. Hence, the piezoelectric patches are supposed to be relatively narrower than the wavelength within interested frequency band of energy harvesting. The wavelength in the central area of the ABH at 5000 Hz is 31 mm herein. The width of piezoelectric patches is set to be 3.5 mm, which can ensure that transducers are relatively narrower than half-wavelengths at frequencies less than 5000 Hz and strains on one single patch are nearly uniformly distributed. Notice that the size of transducers can be determined through optimization analysis for maximum harvested energy subsequently. In order to evaluate the concentration of vibration in the ABH beam, the mean square velocity is defined as follows.

$$\left\langle V^2 \right\rangle = \frac{1}{l}\int_{x_1'}^{x_1} v^2 dx. \tag{7}$$

where v is the velocity of vibration at position x.

Table 1
Geometrical and material properties of the ABH beam.

Geometrical parameters			Material parameters		
ε	0.00012 mm^{-1}	Constant	E	200 GPa	Young's modulus
m	2	power exponent	ρ	7850 kg/m^3	density
h_0	0.5 mm	residual thickness	η	0.005	loss factor
L	430 mm	length of the beams	μ	0.3	Poisson's ratio
x_0–x_p	5 mm	half length of the platform			
x_1–x_0	50 mm	length of the ABH portion			
d	25 mm	length of the distance			
l	110 mm	length of the single ABH			
w_b	22 mm	width of the beam			
h_b	7 mm	thickness of the uniform beam			

Table 2
Geometrical and material properties of piezoelectric patches.

Geometrical parameters			Material parameters		
w_{PZT}	3.5 mm	width of PZT patches	$d_{31} = d_{32}$	-2.74×10^{-10} C/N	piezoelectric matrix
l_{PZT}	22 mm	length of PZT patches	d_{33}	5.93×10^{-10} C/N	
h_{PZT}	0.2 mm	thickness of PZT patches	$d_{24} = d_{15}$	7.41×10^{-10} C/N	
			$E_{11} = E_{22}$	127.21 GPa	elasticity matrix
			E_{12}	80.21 GPa	
			$E_{13} = E_{23}$	84.67 GPa	
			E_{33}	117.44 GPa	
			$E_{44} = E_{55}$	22.99 GPa	
			E_{66}	23.47 Gpa	
			ρ_{PZT}	7500 kg/m^3	density
			εs 11 = εs 22	$1704.4\varepsilon_0$	relative permittivity
			εs 33	$1433.6\varepsilon_0$	

3. Numerical analyses

In order to compare the energy harvesting performance of the ABH beam and the conventional beam, both the transient excitation, similar to an impulse, and the steady-state harmonic excitation were considered. These two types of excitation are the two extreme forms of excitation in their regularity. The excitation in a real energy harvesting system is usually very complicated and has the property between them. In transient excitation, the same amplitude of displacement excitation was used for the two types of beams. In steady-state excitation, the same harmonic force of 3.3 N in amplitude was used for excitation of both the uniform beam and ABH beam at their free end. The sweeping frequency band is from 50 Hz to 5000 Hz. The steady-state analysis was used to reveal the broadband harvesting performance of the ABH system.

3.1. Transient analysis

Since most of the mechanical vibrations in practice are broadband and random, it is necessary to analyze the energy harvesting performance under transient excitation. Understanding of the wave trapping process of the ABH, especially in the presence of geometrical and manufacturing uncertainties, is very important. In this paper, the transient state analysis is used first to research the wave propagation mechanism. Considering the spectrum of the instantaneous vibration sources in practice is mainly distributed in the low frequency band within 5000 Hz, the excitation source used in the simulation is a Gauss-windowed tone burst with a center frequency of 2000 Hz and the bandwidth is about 2500 Hz. In order to excite the structure effectively, a prescribed displacement rather than an excitation force is uniformly applied on the right-hand side edge to generate plane waves in the numerical simulation model. This driving method can be recognized as a simplification of the acceleration excitation in mechanical structures such as vehicles and machine tools. The normalized displacement excitation waveform is shown in Fig. 5 and the corresponding Fourier spectrum is shown in Fig. 6. Obviously, it has the wideband characteristic. The amplitude of the displacement excitation applied on the beam is 10^{-5} meter.

In order to reduce the computation load, the half-width model with symmetrical boundary condition at the center line were used in the transient analysis of both the ABH beam and the reference beam. The half-width model does not change the wave propagation characteristics in ABHs, but it is more computationally efficient. The left-hand sides of both the ABH beam and the uniform beam are fixed and a same displacement excitation load is applied at their free ends. The simulation process was divided into two steps. The excitation is applied for 1.2 ms in the first step. Next, the free vibration of the

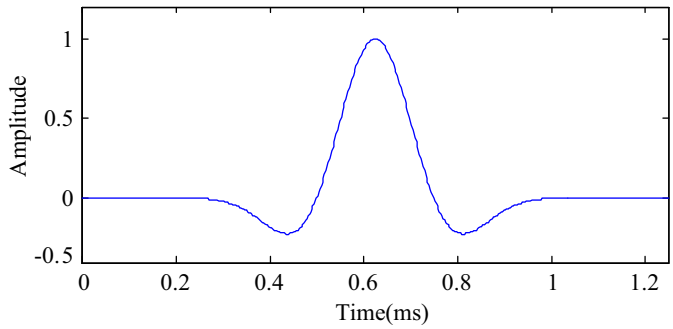

Fig. 5. Normalized displacement excitation waveform.

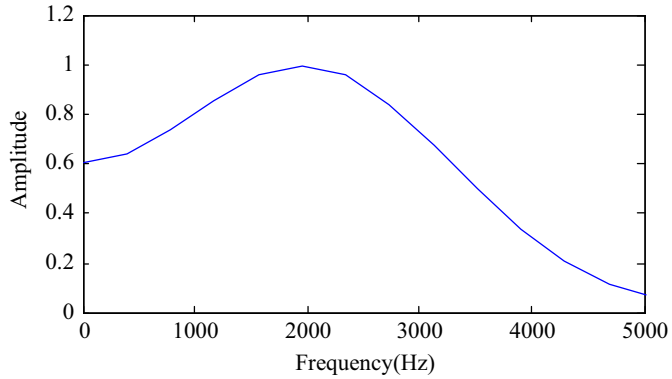

Fig. 6. Normalized displacement excitation waveform Fourier spectrum.

cantilever beam is analyzed in the second step, which continues for 8.8 ms. Each piezoelectric transducer is connected to a resistor of 2000 Ω and the total power in all the resistors is calculated and defined as the harvested power.

Fig. 7 shows the harvested power of two systems under transient excitations. Obviously, the harvested power of the ABH beam is much higher until 4 ms than the reference beam. This can be attributed to strain energy concentration in the ABH area. Fig. 8 shows the normal strain tensor distribution at 1.5 ms in the ABH beam and reference beam. As previously discussed, flexural waves slow down when propagating through the ABH regions, creating high strain energy density areas due to the ABH effect. On the contrary, vibration energy is uniformly distributed in the uniform beam. Figs. 9 and 10 show the voltages on the electrodes of the piezoelectric transducers bonded on the upper surfaces of the ABH beam and the uniform beam, respectively. It is obvious that the voltages generated by the transducers mounted on the ABH beam are much higher compared to the traditional beam, which indicate that mechanical energy can be converted more effectively when using the ABH effect. Besides, the voltage polarity of different patches could be different, which reveals that the width of transducers should not be larger than half the local wavelength of elastic wave due to the cancelling effect. It can also be found from Fig. 7 that the harvested power from the ABH beam decreases very fast to the same level as that of the uniform beam in about 5 ms. This phenomenon can be explained based on the variation of vibration level in the ABH beam.

In order to gain additional insight into the mechanism of higher harvested power and also its fast decrease in ABH beam, the mean square velocities, as defined in Eq. (7), in the three ABHs are calculated and shown in Fig. 11. Fig. 12 compares the mean square velocity of the same regions in the uniform beam. The vibration level of each tapered area reflects the energy concentration performance of the corresponding ABH. As the elastic wave propagates from the free end to clamped, the wave passes sequentially through ABH #3, ABH #2 and finally ABH #1. It is obvious that the ABH beam and the uniform beam exhibit different properties. The maximum value of the mean quadratic velocity in the three ABHs decreases sequentially and the maximum value in ABH #1 is much smaller than that in ABH #3. It means that when the wave propagates through

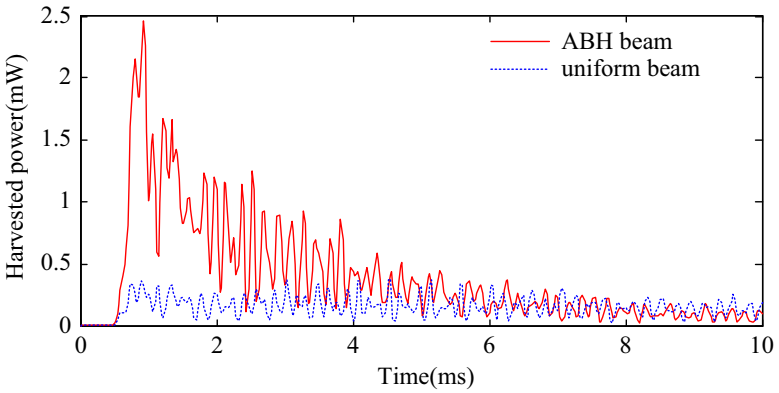

Fig. 7. Harvested power under transient excitations.

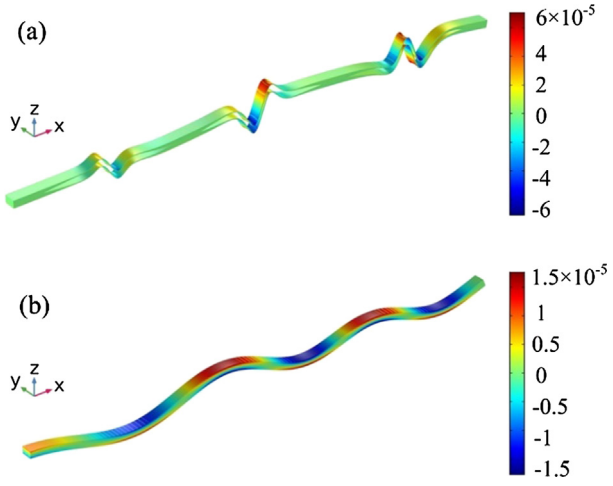

Fig. 8. Distribution of normal strain tensor ε_{xx} at 1.5 ms in (a) ABH beam; (b) uniform beam.

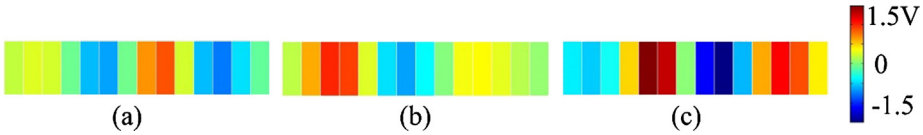

Fig. 9. Voltages of electrodes on the upper surfaces of the ABH beam at 1.5 ms: (a) #1 PZT array; (b) #2 PZT array; (c) #3 PZT array.

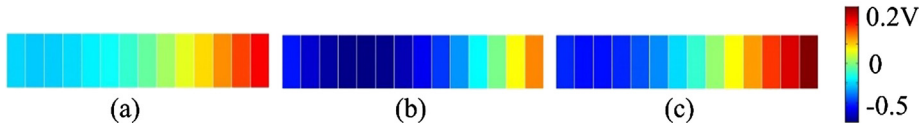

Fig. 10. Voltages of electrodes on the upper surfaces of the uniform beam at 1.5 ms: (a) #1 PZT array; (b) #2 PZT array; (c) #3 PZT array.

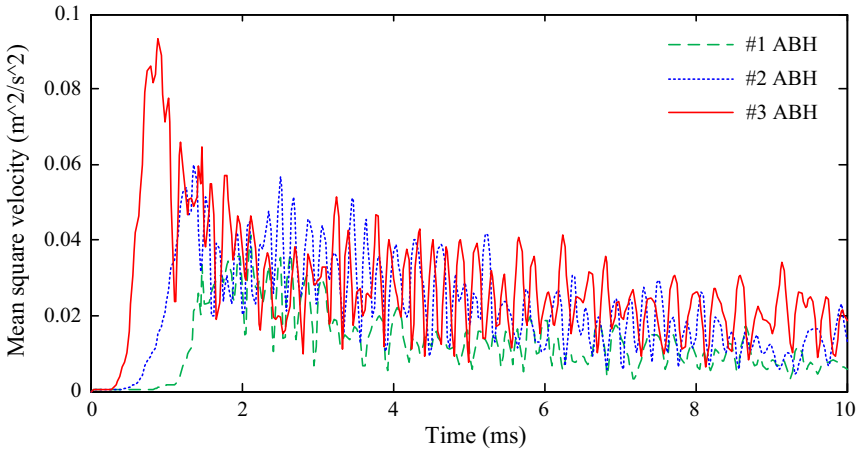

Fig. 11. Mean quadratic velocity of three ABHs.

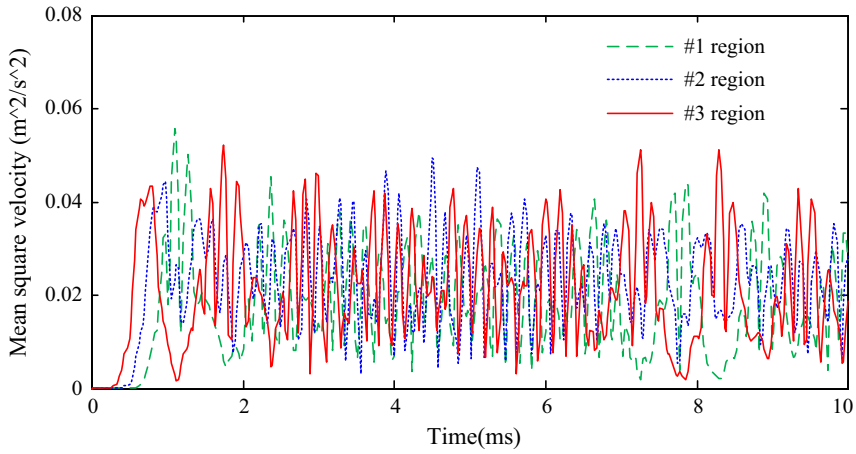

Fig. 12. Mean quadratic velocity of three regions in the uniform beam.

an ABH, the wave energy is efficiently converted to electrical energy in the ABH area and its magnitude decreases significantly. On the contrary, the vibration energy decreases very slowly from region #3 to region #1 in the uniform beam, as shown in Fig. 12, due to low energy conversion efficiency in these regions.

After arriving at the left-hand side edge, the wave packet will reflect back and propagate towards the free edge again. Owing to the transient characteristic of excitation, no standing wave will be formed in both beams. Each time the wave passes the regions with piezoelectric patches, energy conversion is induced. Due to energy concentration in the ABH areas, the harvested power of the ABH beam is higher and also decreases fast than that of the uniform beam.

Fig. 13 shows the average harvested power within 10 ms of each transducer arrays respectively. Results confirm that the ABH effect can provide a significant increase in the harvested power due to high energy concentration performance under transient broadband excitation conditions, while the harvesting performance of the uniform beam is limited because the strain energy density is relatively uniformly distributed. It can also be seen that the harvested power at the PZT array #3 is the highest and that of the PZT array #1 is the lowest, while the harvesting performance of different arrays in the uniform is almost the same.

3.2. Steady state analysis

The steady state analysis can reveal the frequency characteristics of the harvesting performance, which is also very important for an energy harvesting system. In the numerical analysis, the left end of both the ABH beam and the uniform beam are fixed and a harmonic force with an amplitude of 3.3 N is applied to their free end. The frequency is swept from 50 to 5000 Hz and their vibration response and the harvested power are calculated at each frequency.

3.2.1. Dynamic characteristics and energy distribution

In order to demonstrate the ABH effect and quantify the energy concentration performance, the ABH beam is divided into two sets of regions in the length direction, the set of ABH regions and the set of non-ABH regions. The mean quadratic velocities of the beam in these two set of regions, $\left\langle V^2 \right\rangle_{\mathrm{ABH}}$ and $\left\langle V^2 \right\rangle_{\mathrm{non-ABH}}$, were calculated and their ratio is defined as follows:

$$\Gamma = 10\log\frac{\left\langle V^2 \right\rangle_{\mathrm{ABH}}}{\left\langle V^2 \right\rangle_{\mathrm{non-ABH}}} \tag{8}$$

The ratio Γ is also calculated for the uniform beam using the same sets of regions. Fig. 14 shows the energy ratio Γ of both the ABH beam and the uniform beam at different frequency.

Obviously, the index Γ can be used to evaluate the distribution of vibration energy in the two beams. For the ABH beam, the value of Γ is always positive above 300 Hz. Most of the peak values in the considered frequency range is larger than 5. It means the average kinetic energy in the ABH regions is larger than that in the non-ABH regions due to the ABH effect. The peaks in the curve of Γ of the ABH beam correspond to the local resonance modes in the ABH beam. For the uniform beam, the value of Γ fluctuates around 0. The value of Γ of the uniform beam mainly depends on the shape of modal function.

To obtain additional insight into the energy focusing effect, the amplitude of vibration of the two beams at a randomly selected frequency of 3500 Hz is calculated and the results are shown in Fig. 15. Obviously the deformation in the ABH beam is mainly concentrated in the ABH regions, but that in the uniform beam is relatively uniformly distributed. The amplitude of vibration in the ABH region is much larger than that of the uniform beam.

The output voltages of all the piezoelectric patches connected to resistors of 1000 Ω are also calculated and shown in Figs. 16 and 17, respectively, for the ABH beam and uniform beam. The largest output voltage from the ABH beam is about one order greater than that from the uniform. The above results exhibited the energy concentration performance of ABH structure for energy harvesting under steady-state harmonic excitation. Because the energy concentration in ABH structure

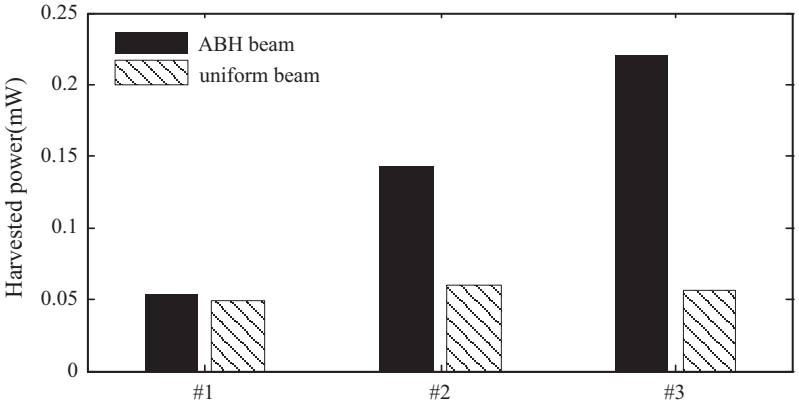

Fig. 13. Average harvested power under transient excitations.

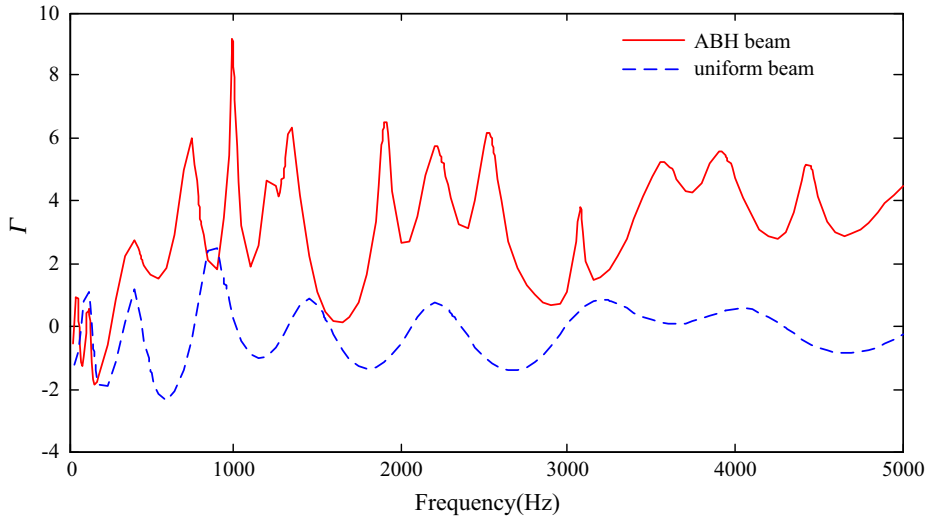

Fig. 14. Ratio of mean quadratic velocity of the ABH portion to the uniform beam portion. PZT patches are under the open-circuit condition.

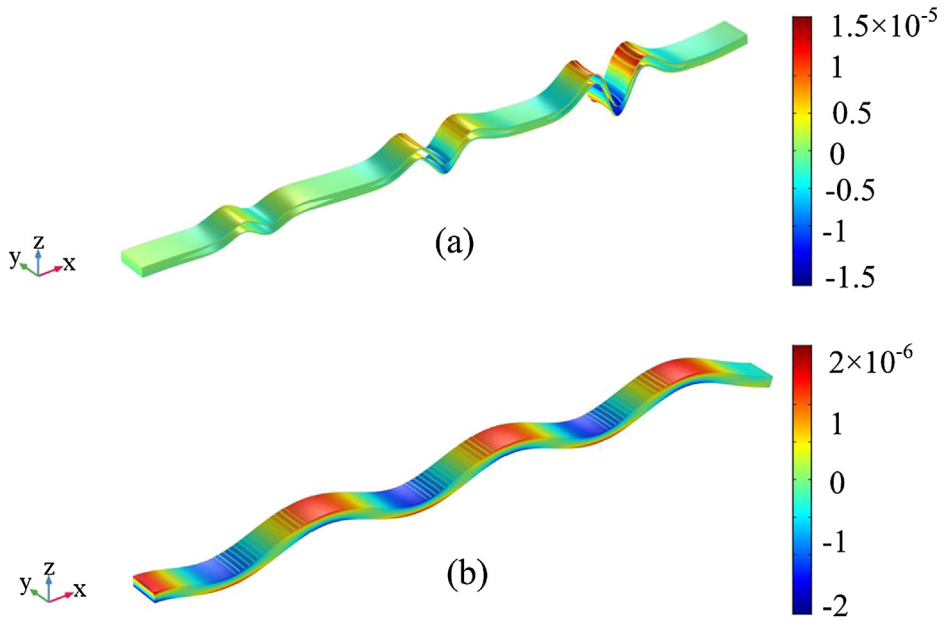

Fig. 15. Distribution of normal strain tensor ε_{xx} at 3500 Hz in (a) ABH beam; (b) uniform beam. PZT patches are under the open-circuit condition.

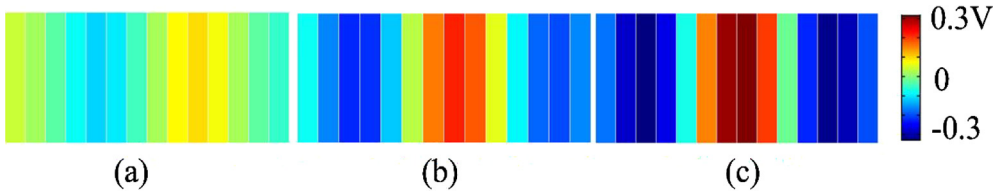

Fig. 16. Voltages of electrodes on the upper surfaces of the ABH beam at 3500 Hz when R = 1000 Ω: (a) #1 ABH; (b) #2 ABH; (c) #3 ABH.

induced by local resonance vibration, the effect can be achieved at the natural frequency of the modes with large local deformation, which is usually much smaller than the characteristic frequency, defined by

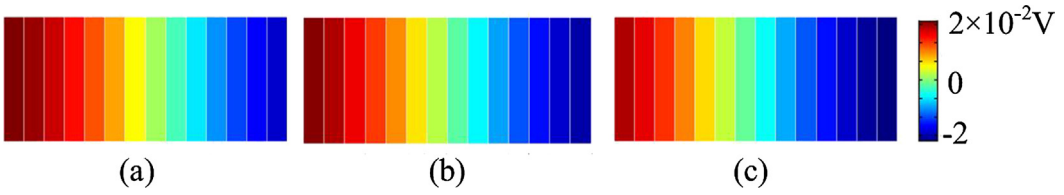

Fig. 17. Voltages of electrodes on the upper surfaces of the uniform beam at 3500 Hz when R = 1000 Ω: (a) #1 PZT array; (b) #2 PZT array; (c) #3 PZT array.

$$f_c = \frac{\pi h_{beam}}{l_{ABH}^2}\sqrt{\frac{E_{beam}}{12\rho_{beam}}} \tag{9}$$

at which the wavelength of the flexural wave equals the characteristic size of the ABH [11].

3.2.2. Comparison of energy harvesting performance

According to Eq. (6), the harvested power is a function of the circular frequency ω, load resistance R, equivalent capacitance C_p, and generated charge Q. The generated charge Q is proportional to the strain, which is determined by the amplitude of vibration. In the modal space, the charge generated by a specific mode can be expressed as $Q = \alpha u_M$, where u_M is the amplitude of the mode and α is the coefficient. If the amplitude of vibration displacement is kept constant, Q is constant. With the assumption of constant charge Q, the optimal resistance can be easily derived from Eqs. (5) and (6) and written as

$$R_{opt} = \frac{1}{\omega C_p} \tag{10}$$

According to the parameters in Table 2, the equivalent capacitance is $C_p \approx 4.88$ nF. Substitution of C_p into the above equation gives

$$R_{opt} \approx \frac{3.26}{f} \times 10^6$$

The above equation indicates that when f = 1000 Hz, the optimal resistance is about 32.6 kΩ.

However, in the case of force excitation with constant amplitude, the amplitude of vibration is affected by the harvested energy because extraction of energy by the harvesting system increases the structural damping. It means that the amplitude of vibration u_M cannot be considered as constant. The amplitude during energy harvesting is smaller than that without energy harvesting. Hence, the optimal resistance R_{opt} for constant force excitation may be smaller. When the coefficient α is great enough, there may not exist optimal resistance.

The harvested power of both the ABH beam and the uniform beam is calculated when the resistance is changed from 100 Ω to 100 kΩ and the results are shown in Figs. 18 and 19. Overall in the considered frequency range and the range of load resistance, the harvested power of the ABH beam is significantly larger than that of the uniform beam. Frequency

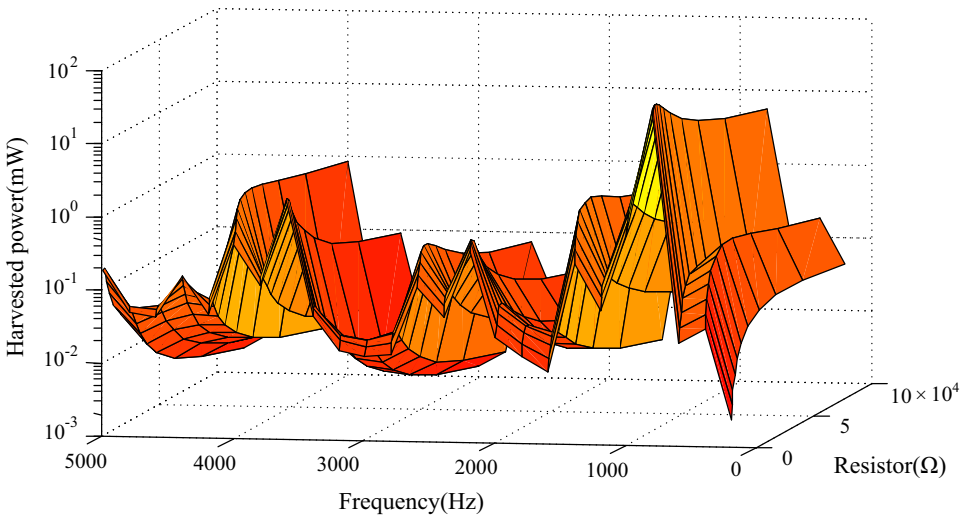

Fig. 18. Harvested power of the ABH beam as a function of frequency and load resistor.

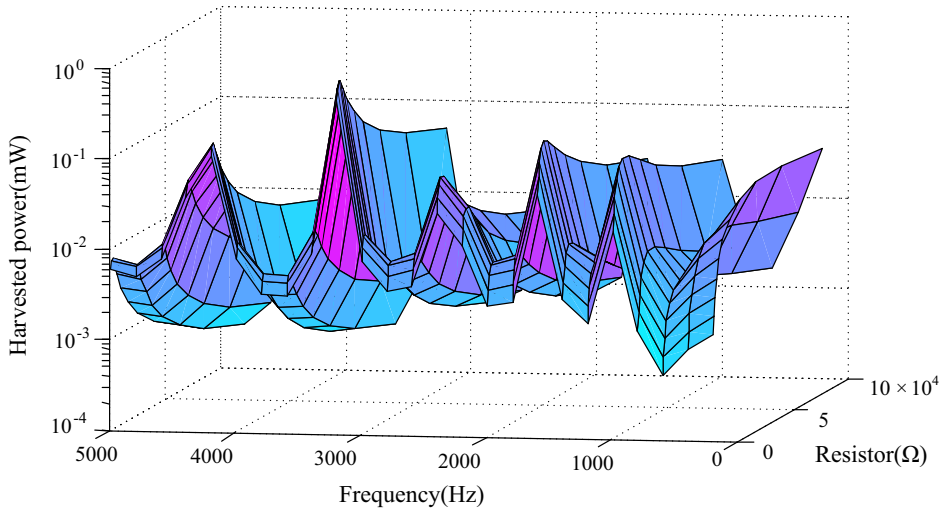

Fig. 19. Harvested power of the uniform beam as a function of frequency and load resistor.

has stronger influence on the harvested power than the load resistance. This is because the resonant vibration usually is larger than the non-resonant vibration. It can also be seen that at some of the resonance frequencies, there is an optimal resistance with maximum harvested power. However, at some resonance frequency, the power decreases monotonically in the considered resistance range. It can be attributed to large value of coefficient α due to strong electromechanical coupling at these modes.

Fig. 20 shows the harvested power as a function of frequency when the resistance is 1000 Ω. There are many peaks in the curved of the harvested power of both beams. The peak frequencies correspond to the resonance frequencies of the two beams. The harvested power of the ABH beam is systematically larger than that of the uniform beam though at some resonance frequencies the power of the uniform beam can exceed that of the ABH beam. At the non-resonance frequencies, the power of the ABH beam is larger than that of the uniform beam because the ABH beam has higher modal density than the uniform structure.

The ABH beam is especially advantageous for energy harvesting in the frequency as shown in Eq. (10). This can be attributed to the energy concentration performance of the ABH beam. But at low frequency, ABH beam still has higher energy harvesting performance than the uniform beam. For better explanation, the first two modal functions of the ABH beam are calculated and shown in Fig. 21 to illustrate its energy concentration characteristic. High level of deformation and strain values in the ABH regions directly leads to high voltages on the electrodes, as shown in Figs. 22 and 23, which makes the harvesting effective at lower frequencies. The above results also show that the ABH beam can extend operating frequency band as well as increase the harvested power remarkably.

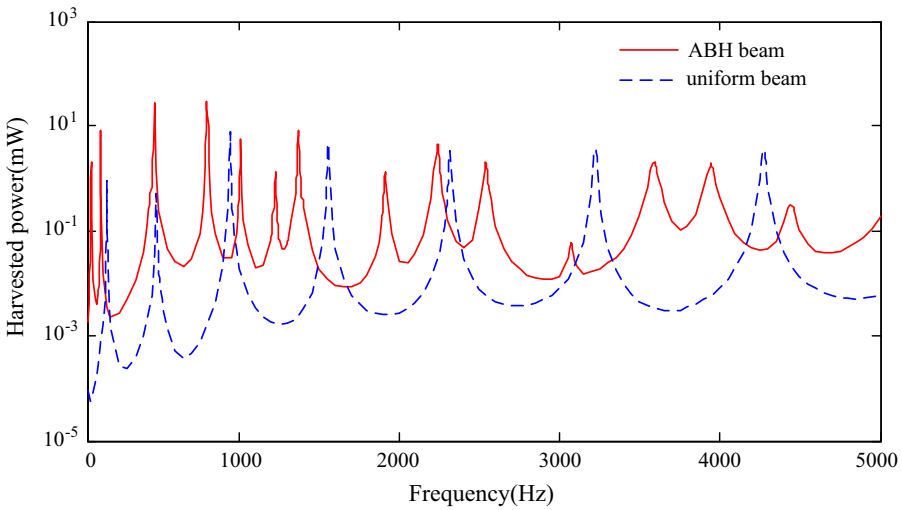

Fig. 20. Harvested power as a function of frequency when $R = 1000\ \Omega$.

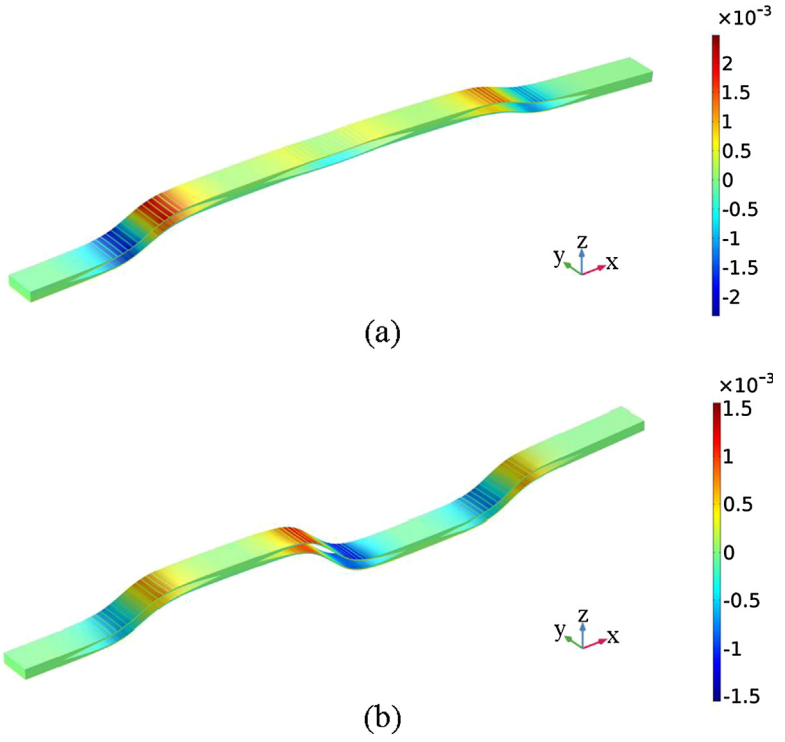

Fig. 21. Distribution of normal strain tensor ε_{xx} in the ABH beam: (a) 78 Hz; (b) 138 Hz.

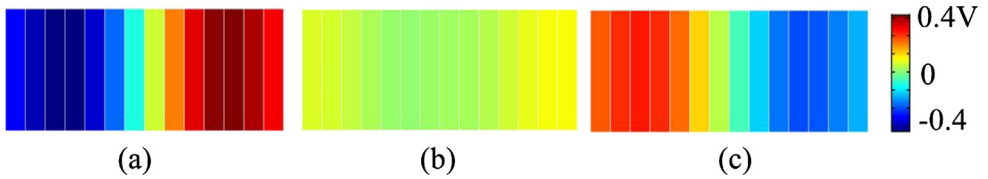

Fig. 22. Electrical potential of electrodes on the upper surfaces of the ABH beam with separated patches at 78 Hz: (a) #1 ABH; (b) #2 ABH; (c) #3 ABH.

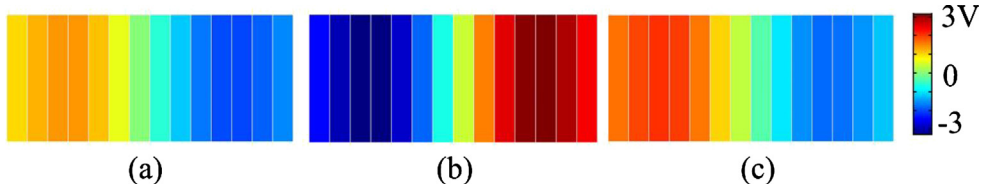

Fig. 23. Electrical potential of electrodes on the upper surfaces of the ABH beam with separated patches at 138 Hz: (a) #1 ABH; (b) #2 ABH; (c) #3 ABH.

3.2.3. Influence of the transducers dimension on harvesting performance

In this study, three array of 14 piezoelectric transducers were bonded on each side of the beams to improve the efficiency of energy harvesting. An array of small transducers, instead of a uniform piezoelectric patch, was used to avoid cancellation of positive and negative charges generated due to alternative modal strain at different positions. In order to investigate the influence of the transducer dimensions on the energy harvesting performance, three uniform PZT patches were bonded in the same ABH areas on each side of the ABH beam. Due to the higher stiffness of single PZT patches, the resonance frequency of the new beam with uniform piezoelectric patches is higher. For fair comparison, the generated voltage at the same structural mode, with resonance frequencies of 4073 Hz and 3999 Hz respectively for the two, is considered.

Figs. 24 and 25 present electrical potential on the surface of the transducers when the influence of electrodes are neglected. The potential is a linear function of the local strain so that it is non-uniform on the same patch. When a single uniform piezoelectric patch is bonded in an ABH area, there are regions of positive potential and regions of negative ones.

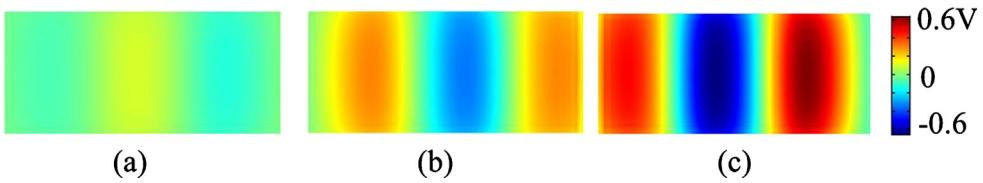

Fig. 24. Electrical potential field of transducers on the upper surfaces of the ABH beam with three single patches at 4073 Hz: (a) #1 ABH; (b) #2 ABH; (c) #3 ABH.

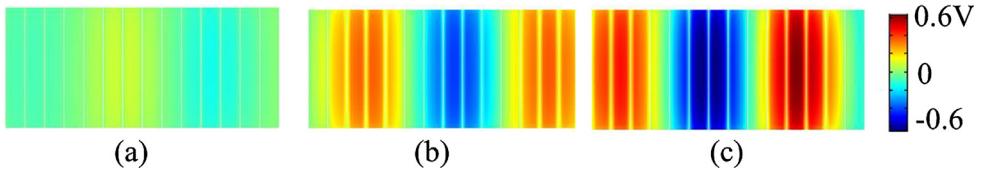

Fig. 25. Electrical potential field of transducers on the upper surfaces of the ABH beam with separated patches at 3999 Hz: (a) #1 ABH; (b) #2 ABH; (c) #3 ABH.

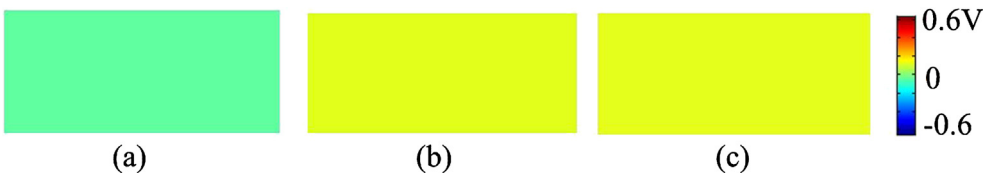

Fig. 26. Electrical potential of electrodes on the upper surfaces of the ABH beam with three single patches at 4073 Hz: (a) #1 ABH; (b) #2 ABH; (c) #3 ABH.

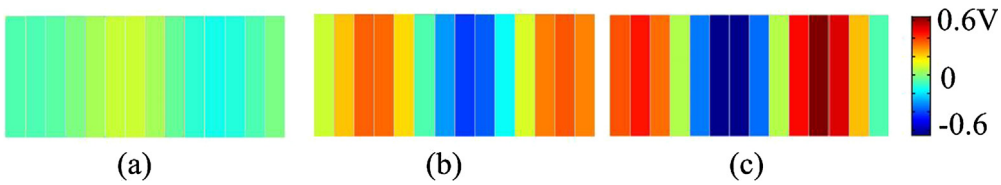

Fig. 27. Electrical potential of electrodes on the upper surfaces of the ABH beam with separated patches at 3999 Hz: (a) #1 ABH; (b) #2 ABH; (c) #3 ABH.

The wavelength of the vibration mode at this frequency is 34.6 mm, but the single uniform piezoelectric transducer is 50.4 mm. Therefore, there are regions of both positive and negative normal strain ε_x in the transducer area. Figs. 26 and 27 compare the voltages on the electrodes of piezoelectric patches on the two beams. Obviously the voltage on single uniform piezoelectric transducer is very small due to cancellation of positive and negative electrical potential. However, the voltages on the electrodes of the small transducers are almost the same as their local electrical potential. Division of large uniform piezoelectric transducer into an array of small transducer can significantly increase the energy harvesting efficiency though it also increases the complexity of the harvesting system.

4. Experimental validations of harvesting performance

An experimental setup was developed to further verify the predicted harvesting performance of the system. A double-layered tapered beam with three embedded ABHs and a uniform beam were fabricated. Both them have the same material parameters and geometrical configurations with the structures built in the numerical simulation. Three 1×14 piezoelectric patches arrays were mounted on the upper surface of each ABH respectively. The attached piezoelectric patches were designed to have the same dimensions and material parameters with transducers used for the numerical study. Two electrodes of each transducer were fixed on the upper surface for ease of welding. Each transducer was shunted with a separate resistor of 10kΩ.

Both the left-hand side edges of two test structures were clamped to achieve fixed-free boundary conditions, as shown in Fig. 28. The free edges were excited by a shaker (YMC VT-50) generating an excitation in the out-of-plane direction. A force transducer (PCB 208C02) connecting the shaker with the structure was utilized to measure the excitation force signal. The

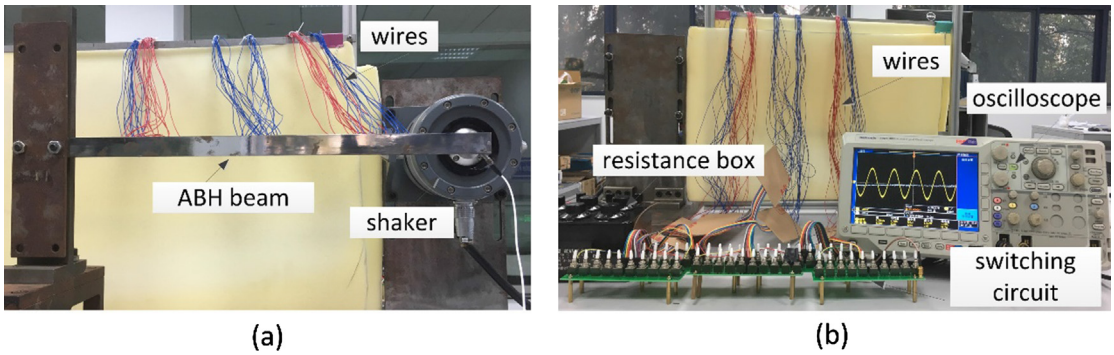

Fig. 28. Experimental set-up: (a) the front side; (b) the back side.

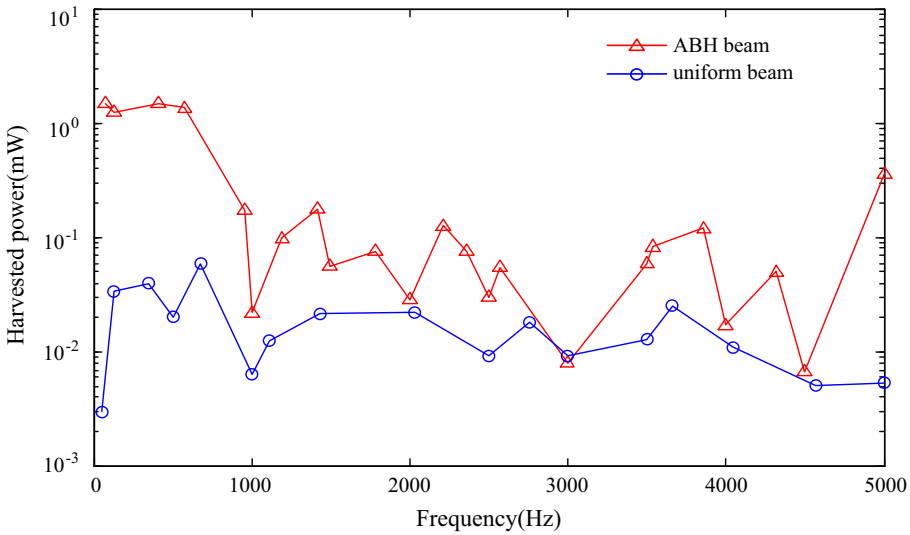

Fig. 29. Harvesting power under steady state.

vibration responses were measured by a Polytec^{TM} laser scanning vibrometer (PSV 400). The electrical voltage of each resistor was measured via a oscilloscope (MSO3032), whose input impedance is 10MΩ.All the wires are suspended to reduce the effect of the added mass on the vibration characteristics of the primary structure. In order to assess the broadband harvesting performance of the test structures, the harvesting power under modal frequencies and frequencies between 500 Hz and 5000 Hz with a step of 500 Hz are measured. The excitation force was set to be 3.3 N constantly under different frequencies.

Fig. 29 provides a comparison of the harvested power between the ABH beam and uniform beam under steady-state excitation. It can be seen that the overall trend of the experimental results is consistent with the simulation ones. The harvested power of the ABH beam is systematically larger than that of the compared with the uniform beam; particularly at some frequencies, the harvesting performance is increased 10 times by embedding ABHs into the beam. But at some frequencies, the harvested power is barely enhanced. This is mainly due to the different resonance frequencies of the two beams. The resonance peaks in the experimental curves of both the beams are not as sharp as those of the simulation curves. This phenomenon can be attributed to two reasons. The first reason is that the resonance peaks can rarely be captured in the small number of experimental points in frequency response curve. The second reason is that the modal damping ratios of the experimental system is larger than those in the simulation due to damping loss in the bonding materials and wirings of the piezoelectric transducers. In summary, embedding ABHs into a beam structure can significantly boost the power of energy harvesting over a wide frequency band.

5. Conclusions

In this paper, a fully coupled simulation model was established to estimate the vibration-based energy harvesting performance of a compound ABH beam. The ABH effect allows an effective reduction of wave speed, which forms a confined area with high energy density over a wide frequency band. The harvested power can be substantially boosted through the depo-

sition of PZT patches in the energy concentration zones compared to the case of the uniform beam. Since the energy focalization is a broadband phenomenon, harvesting with ABH features is still effective when applied to a non-resonant steady-state, which solves the limitation of traditional vibration-based energy harvesting systems effectively. The piezoelectric patches were designed to be relatively narrower than the wavelength in ABHs, making it adaptable to avoid the charge converted being neutralized in a large frequency range. Results reveal that the ABH feature mounted with transducers allows the effective conversion and absorption of mechanical energy during both steady state and transient excitation. Experiments confirmed that the compound ABH feature offers much better harvesting performance than the uniform beam. The energy harvesting circuit connected to each piezoelectric patch was simply represented by a separate resistor in the finite element model. This can be optimized by integrated circuit to combine all the patches together with only one harvesting circuit to enhance the harvesting performance. In addition, the coupling effects between the resistors and the ABH features are of great significance in the optimal design and need to be further investigated in the future work. To sum up, the proposed design of energy harvesting system using ABH features can obtain much more effective harvesting performance over a wide frequency band.

Acknowledgements

This research was supported by National Natural Science Foundation of China, China (No. 11532006 & 51775267; Natural Science Foundation of Jiangsu Province, China (BK20181286); Fundamental Research Funds for the Central Universities, China (No. NE2015001); Equipment Pre-research Foundation, China (No. 61402100103); A Project Funded by the Priority Academic Program Development of Jiangsu Higher Education Institutions, China.

References

[1] M.A. Mironov, Propagation of a flexural wave in a plate whose thickness decreases smoothly to zero in a finite interval, Sov. Phys. Acoust. 34 (1988) 318–319.
[2] V.V. Krylov, F.J.B.S. Tilman, Acoustic 'black holes' for flexural waves as effective vibration dampers, J. Sound Vib. 274 (2004) 605–619.
[3] D.J. O'Boy, V.V. Krylov, V. Kralovic, Damping of flexural vibrations in rectangular plates using the acoustic black hole effect, J. Sound Vib. 329 (2010) 4672–4688.
[4] V.V. Krylov, New type of vibration dampers utilising the effect of acoustic'black holes', Acta Acustica United with Acustica 90 (2004) 830–837.
[5] V.V. Krylov, R.E.T.B. Winward, Experimental investigation of the acoustic black hole effect for flexural waves in tapered plates, J. Sound Vib. 300 (2007) 43–49.
[6] E.P. Bowyer, V.V. Krylov, Sound radiation of rectangular plates containing tapered indentations of power-law profile, in: Proceedings of Meetings on Acoustics 164ASA, ASA, 2012, p. 030002.
[7] A. Azbaid El Ouahabi, V. Krylov, D. O'boy, Experimental investigation of the acoustic black hole for sound absorption in air, Proceedings of the 22nd International Congress on Sound and Vibration, Florence, Italy, 12th-16th July, International Institute of Acoustics and Vibration, 2015.
[8] A.A. El-Ouahabi, V.V. Krylov, D.J. O'Boy, Investigation of the acoustic black hole termination for sound waves propagating in cylindrical waveguides, INTER-NOISE and NOISE-CON Congress and Conference Proceedings, Institute of Noise Control Engineering, 2015, pp. 636-645.
[9] L. Tang, L. Cheng, H. Ji, J. Qiu, Characterization of acoustic black hole effect using a one-dimensional fully-coupled and wavelet-decomposed semi-analytical model, J. Sound Vib. 374 (2016) 172–184.
[10] H. Ji, J. Luo, J. Qiu, L. Cheng, Investigations on flexural wave propagation and attenuation in a modified one-dimensional acoustic black hole using a laser excitation technique, Mech. Syst. Sig. Process. 104 (2018) 19–35.
[11] W. Huang, H. Ji, J. Qiu, L. Cheng, Wave energy focalization in a plate with imperfect two-dimensional acoustic black hole indentation, J. Vib. Acoust. 138 (2016), 061004–061004-061012.
[12] B.M.P. Chong, L.B. Tan, K.M. Lim, H.P. Lee, A review on acoustic black-holes (ABH) and the experimental and numerical study of ABH-featured 3D printed beams, Int. J. Appl. Mech. 9 (2017) 1750078.
[13] E.P. Bowyer, V.V. Krylov, A review of experimental investigations into the acoustic black hole effect and its applications for reduction of flexural vibrations and structure-borne sound, (2015).
[14] O. Prill, R. Busch, Finite Element Simulations of Acoustic Black Holes as Lightweight Damping Treatments for Automotive Body Panels with Application to Full Vehicle Interior Wind Noise Predictions, INTER-NOISE and NOISE-CON Congress and Conference Proceedings, Institute of Noise Control Engineering, 2016, pp. 5210-5221.
[15] L. Zhao, S.C. Conlon, F. Semperlotti, Broadband energy harvesting using acoustic black hole structural tailoring, Smart Mater. Struct. 23 (2014) 065021.
[16] L. Zhao, S.C. Conlon, F. Semperlotti, An experimental study of vibration based energy harvesting in dynamically tailored structures with embedded acoustic black holes, Smart Mater. Struct. 24 (2015) 065039.
[17] N.H. Schiller, S.-C.S. Lin, R.H. Cabell, T.J. Huang, Design of a variable thickness plate to focus bending waves, INTER-NOISE and NOISE-CON Congress and Conference Proceedings, Institute of Noise Control Engineering, 2012, pp. 8951-8958.
[18] T. Zhou, L. Tang, H. Ji, J. Qiu, L. Cheng, Dynamic and static properties of double-layered compound acoustic black hole structures, Int. J. Appl. Mech. 9 (2017) 1750074.
[19] H.H. Law, P.L. Rossiter, G.P. Simon, L.L. Koss, Characterization of mechanical vibration damping by piezoelectric materials, J. Sound Vib. 197 (1996) 489–513.
[20] K. Yi, M. Collet, S. Chesne, M. Monteil, Enhancement of elastic wave energy harvesting using adaptive piezo-lens, Mech. Syst. Sig. Process. 93 (2017) 255–266.
[21] Z. Chen, Y. Yang, Z. Lu, Y. Luo, Broadband characteristics of vibration energy harvesting using one-dimensional phononic piezoelectric cantilever beams, Physica B 410 (2013) 5–12.
[22] M. Carrara, M. Cacan, M. Leamy, M. Ruzzene, A. Erturk, Dramatic enhancement of structure-borne wave energy harvesting using an elliptical acoustic mirror, Appl. Phys. Lett. 100 (2012) 204105.
[23] M. Carrara, J. Kulpe, S. Leadenham, M. Leamy, A. Erturk, Fourier transform-based design of a patterned piezoelectric energy harvester integrated with an elastoacoustic mirror, Appl. Phys. Lett. 106 (2015) 013907.
[24] M. Carrara, M. Cacan, J. Toussaint, M. Leamy, M. Ruzzene, A. Erturk, Metamaterial-inspired structures and concepts for elastoacoustic wave energy harvesting, Smart Mater. Struct. 22 (2013) 065004.
[25] S.R. Anton, H.A. Sodano, A review of power harvesting using piezoelectric materials (2003–2006), Smart Mater. Struct. 16 (2007) R1.
[26] Y. Wu, J. Qiu, S. Zhou, H. Ji, Y. Chen, S. Li, A piezoelectric spring pendulum oscillator used for multi-directional and ultra-low frequency vibration energy harvesting, Appl. Energy 231 (2018) 600–614.